

Continuous Normalizing Flows for Uncertainty-Aware Human Pose Estimation

Shipeng Liu^[0009–0004–0703–9431], Ziliang Xiong^[0009–0008–8277–7476], Bastian Wandt^[0009–0002–1203–1093], and Per-Erik Forssén^[0000–0002–5698–5983]

Computer Vision Laboratory, Dept of E. E., Linköping University, Sweden
{firstname.lastname@liu.se}

Abstract. Human Pose Estimation (HPE) is increasingly important for applications like virtual reality and motion analysis, yet current methods struggle with balancing accuracy, computational efficiency, and reliable uncertainty quantification (UQ). Traditional regression-based methods assume fixed distributions, which might lead to poor UQ. Heatmap-based methods effectively model the output distribution using likelihood heatmaps, however, they demand significant resources. To address this, we propose Continuous Flow Residual Estimation (CFRE), an integration of Continuous Normalizing Flows (CNFs) into regression-based models, which allows for dynamic distribution adaptation. Through extensive experiments, we show that CFRE leads to better accuracy and uncertainty quantification with retained computational efficiency on both 2D and 3D human pose estimation tasks.

Keywords: Computer Vision · Human Pose Estimation · Continuous Normalizing Flows · Flow Matching.

1 Introduction

Human Pose Estimation (HPE) is a critical task in computer vision with applications spanning virtual reality, motion analysis, and intelligent surveillance. It involves identifying human keypoint locations from visual data. These keypoints correspond to anatomical landmarks such as joints (e.g. shoulders, elbows, and knees). Despite steady improvements, reliable real-world performance remains a challenge due to complexities such as noise, occlusions, and diversity in posture. Addressing these issues requires not only accurate pose estimation but also effective uncertainty quantification to ensure robustness and interpretability in practical scenarios.

Uncertainty Quantification (UQ) is particularly significant in dynamic and unpredictable environments, such as safety-critical applications. Beyond predicting joint coordinates, understanding the uncertainty of the model in its outputs enables error identification, adaptation to abnormal input, and informed decisions on the need for human intervention. However, existing methods often fail to sufficiently address uncertainty estimation.

Two dominant approaches in HPE are regression-based and heatmap-based methods. Regression-based methods [13, 29, 21, 27] directly predict joint coordinates by minimizing loss functions such as ℓ_1 loss (Laplace assumption) or

ℓ_2 (Gaussian assumption). Although computationally efficient, these models are based on fixed distributional assumptions [18], which can lead to suboptimal performance and unreliable uncertainty estimates. For instance, heteroscedastic regression based on Laplace distributions has shown better results compared to Gaussian-based models [13], indicating that real-world joint locations often deviate from Gaussian assumptions.

Heatmap-based methods [28, 24, 8, 22, 19], on the other hand, frame keypoint detection as a classification problem by generating likelihood heatmaps for each keypoint. Although these approaches, such as HRNet [24] and SimplePose [28], achieve high accuracy, they come with significant computational and memory requirements.

To address these limitations, we propose a novel approach that combines the strengths of regression-based methods with Continuous Normalizing Flows (CNFs) [3] shown in Figure 1.

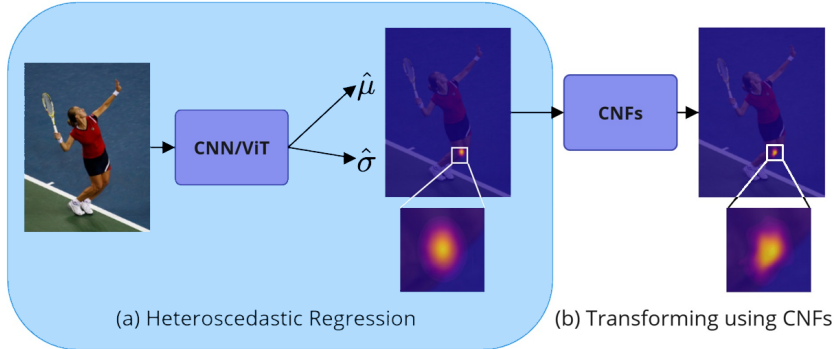


Fig. 1: Overview of our proposed method. Heteroscedastic Deep Regression (Blue box) estimates the mean and scale of keypoint locations, which can be described as a simple distribution (e.g., Gaussian or Laplacian). Our CNF then transforms this into a more complex uncertainty distribution.

A CNF uses neural ordinary differential equations to learn complex data distributions without fixed assumptions, using continuous-time transformations. The resulting framework, Continuous Flow Residual Estimation (CFRE), integrates a prior regression network with CNFs to estimate joint locations and associated uncertainties. During training, the regression network assumes a Laplace distribution, while CNFs dynamically refine the predictions to better align with real-world data. Importantly, the framework incurs no additional computational costs during inference, making it both practical and efficient.

We validate our method on 2D and 3D HPE tasks using MSCOCO [15] and Human3.6M [10], achieving superior performance over traditional regression and heatmap-based models while ensuring calibrated confidence. Qualitative results indicate that the model captures more complex patterns, including anisotropy and sharper peaks than Gaussian distributions. Experimental results on mAP

and AUSE metrics demonstrate that improved data distribution fitting also enhances uncertainty quantification.

Our contributions include:

- **Revealing misalignment:** We show that the misalignment between the distribution assumption in regression models and data distribution leads to less accurate estimates and uncalibrated confidence.
- **Proposing a Novel Method (CFRE):** We introduce CNFs into Human Pose Estimation, and to improve the efficiency of model training, we propose a training regime that decouples the CNFs and the regression network. CNFs dynamically adjust regression parameters during training without adding extra computation during inference. Empirically, our training regime significantly outperforms explicit NLL-based training.

2 Related Work

2.1 Heatmap-based Methods

Heatmap-based approaches were proposed by Tompson *et al.* [26], which utilize likelihood heatmaps to estimate joint locations. Recently, heatmap-based methods [28, 24, 8, 22, 19] have dominated due to their ability to model spatial relationships effectively. Sun *et al.* [24] achieved competitive performance by maintaining the high resolution of image features during forward propagation in CNNs. However, these methods suffer from high computational and storage demands, making them unsuitable for scenarios requiring efficiency, such as edge-device deployments.

2.2 Regression-based Methods

Unlike heatmap-based methods, regression-based approaches [29, 21, 27] prioritize computational efficiency but often lag behind in performance. To estimate the confidence of model predictions, regression-based methods commonly employ heteroscedastic regression [11], which models per-sample variance. However, this approach typically assumes a specific distribution, and deviations from the true data distribution can result in suboptimal performance. Recently, Li *et al.* [13] proposed leveraging normalizing flows (NFs) to model data distributions without relying on specific assumptions. However, the discrete-time transformations in normalizing flows may limit their ability to accurately capture complex data distributions. We adopt continuous normalizing flows, which learn such distributions through continuous-time transformations and have demonstrated superior performance in high-dimensional data generation tasks.

3 Method

In this section, we introduce a novel regression-based framework that integrates CNFs into human pose estimation. This approach addresses the limitations of fixed distributional assumptions by allowing the model to dynamically learn complex data distributions. Additionally, a specialized loss function is designed to enhance both accuracy and uncertainty quantification.

3.1 Regression Paradigm

The proposed model employs a top-down 2D human pose estimation approach. For a given image \mathcal{I} , the model predicts the coordinates of K joints $\hat{\mathbf{p}} \in \mathbb{R}^{K \times 2}$ and their corresponding joint-wise confidence scores $\hat{s} \in [0, 1]^K$. These joint-wise confidence scores are averaged into an instance-wise confidence score $\hat{c} \in [0, 1]$, which represents the overall reliability of the model’s predictions.

The regression paradigm estimates the deterministic coordinates of joints and corresponding scale by modeling the joint distribution $P_\beta(x|\mathcal{I})$ as a probabilistic distribution parameterized by the mean $\hat{\mu}$ and standard deviation $\hat{\sigma}$ using heteroscedastic Deep Regression [11]. Here, β denotes the learnable parameters of the regression model. The distribution is typically assumed to be Gaussian or Laplacian, with the regression model estimating $\hat{\mu}$ and $\hat{\sigma}$ for each joint given an input image \mathcal{I} . We follow the previous work [7] to normalize $\hat{\sigma}$ to the range $[0, 1]$.

To optimize the regression model, the negative log-likelihood (NLL) of the ground truth joint locations μ_g is minimized as follows:

$$\mathcal{L}_{\text{reg}} = -\log P_\beta(x|\mathcal{I}) \Big|_{x=\mu_g}. \quad (1)$$

From the distribution parameters, the predicted joint locations $\hat{\mathbf{p}}$ and confidence scores \hat{s}_k for each joint are obtained as:

$$\hat{\mathbf{p}} = \hat{\mu}, \quad \hat{s}_k = 1 - \hat{\sigma}. \quad (2)$$

However, the fixed assumptions about the joint distributions in traditional regression methods limit their flexibility in adapting to the complex nature of human pose data. To address this issue, we propose integrating CNFs into the regression paradigm.

3.2 Reparameterization

To enable seamless integration of CNFs with regression models and to simplify training, we employ a reparameterization technique based on previous works [13]. The architecture of the proposed method is illustrated in Figure 2.

Here we assume that the underlying joint distributions belong to the same family of density functions but may differ in their means and standard deviations depending on the input \mathcal{I} . The regression model, parameterized by β , predicts the mean $\hat{\mu}$ and standard deviation $\hat{\sigma}$ of the joint locations. Using these predictions, the CNFs, parameterized by θ , transform a simple initial distribution into a complex normalized distribution. $z(t)$ here denotes the state of the transformation at time t , and $f(z(t), t; \theta)$ defines a velocity field parameterized by θ . The process starts from a simple base distribution $z(0) \sim \mathcal{N}(0, I)$ and evolves into a target distribution $z(1) \sim P_\theta(\bar{x})$ by CNFs, that captures the data distribution.

The reparameterized process begins by standardizing the ground truth joint location x as follows:

$$\bar{x} = \frac{x - \hat{\mu}}{\hat{\sigma}}, \quad (3)$$

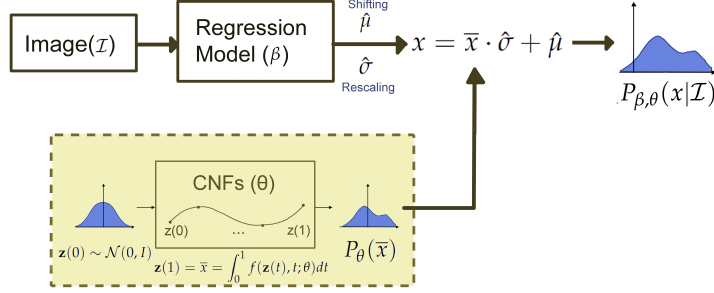


Fig. 2: The proposed CFRE architecture. The yellow box is our contribution.

where $\bar{x} \sim P_\theta(\bar{x})$. Here, $P_\theta(\bar{x})$ represents the distribution learned by the CNFs, and \bar{x} is the standardized residual. The original joint location distribution is reconstructed using:

$$x = \bar{x} \cdot \hat{\sigma} + \hat{\mu} \sim P_{\beta, \theta}(x|\mathcal{I}), \quad (4)$$

where $P_{\beta, \theta}(x|\mathcal{I})$ is the final predicted distribution of the joint location.

3.3 Negative Log-Likelihood Estimation with CNFs

An intuitive way to train the parameters of both the regression model and CNFs is to minimize the negative log-likelihood (NLL) of the predicted joint distribution $P_{\beta, \theta}(x|\mathcal{I})$. The reparameterization introduced earlier allows us to express the NLL as a function of the initial distribution and the CNF transformation dynamics.

Density Transformation via CNFs Using the continuous transformation defined by CNFs, the log-probability of the normalized variable $\bar{x} = \frac{x - \hat{\mu}}{\hat{\sigma}}$, where $\bar{x} \sim P_\theta(\bar{x})$, evolves as follows [3]:

$$\frac{\partial \log P_\theta(z(t))}{\partial t} = -\text{tr} \left(\frac{\partial f(z(t), t; \theta)}{\partial z(t)} \right), \quad (5)$$

where $f(z(t), t; \theta)$ represents the vector field parameterized by θ , and $\text{tr}(\cdot)$ denotes the trace operator. By integrating this differential equation over the interval $[0, 1]$, we obtain:

$$\log P_\theta(\bar{x}) = \log P_\theta(z(0)) - \int_0^1 \text{tr} \left(\frac{\partial f(z(t), t; \theta)}{\partial z(t)} \right) dt. \quad (6)$$

The full joint distribution $P_{\beta, \theta}(x|\mathcal{I})$ is then reconstructed by applying the change-of-variable formula:

$$P_{\beta, \theta}(x|\mathcal{I}) = \frac{1}{\hat{\sigma}} \cdot P_\theta \left(\frac{x - \hat{\mu}}{\hat{\sigma}} \right). \quad (7)$$

Optimizing the NLL By taking the negative log of $P_{\beta,\theta}(x|I)$, we obtain the loss function that we use for training:

$$\mathcal{L}_{\text{NLL}} = \log \hat{\sigma} - \log P_{\theta}(z(0)) + \int_0^1 \text{tr} \left(\frac{\partial f(z(t), t; \theta)}{\partial z(t)} \right) dt. \quad (8)$$

The key computational challenge lies in evaluating the trace term, which involves the Jacobian of the vector field and is computationally expensive.

Trace Estimation with the Hutchinson Trace Estimator (HTE). To mitigate the computational burden, we use the Hutchinson estimator [6], which approximates the trace of a matrix through stochastic sampling:

$$\text{tr} \left(\frac{\partial f(z(t), t; \theta)}{\partial z(t)} \right) \approx \mathbb{E}_{\varepsilon \sim \mathcal{N}(0, I)} \left[\varepsilon^\top \frac{\partial f(z(t), t; \theta)}{\partial z(t)} \varepsilon \right], \quad (9)$$

where ε is a random vector sampled from a standard normal distribution.

3.4 Training of the Model

The proposed training approach optimizes both the regression network and Continuous Normalizing Flows (CNFs) in an end-to-end manner. However, while the HTE efficiently approximates the trace of the Jacobian matrix, it introduces variance. This can lead to non-smooth loss curves and convergence difficulties. In addition, the numerical integration may also introduce errors.

Decoupled Training Strategy To address these issues, we propose a decoupled training strategy of the regression network and CNFs. The total loss function is decomposed as:

$$\mathcal{L}_{\text{total}} = \mathcal{L}_{\text{reg}} + \lambda(\hat{\sigma}) \cdot \mathcal{L}_{\text{flow}}, \quad (10)$$

where

$$\lambda(\hat{\sigma}) = c \cdot (1 - \hat{\sigma}), \quad (11)$$

is the self-adaptive scaling factor and c is a hyperparameter. Here \mathcal{L}_{reg} trains the regression network to fit a reference distribution, while $\mathcal{L}_{\text{flow}}$ refines the reference by modeling residuals via CNFs and enables the regression network to adapt to the new data distribution during training, leading to more precise scale estimation.

Self-adaptive scaling factor $\lambda(\hat{\sigma})$ adjusts the influence of CNFs component based on the uncertainty, $\hat{\sigma}$, of the predictions of the regression network. We notice that during the early training epochs, CNFs are not yet well-trained, hence downweighting by the self-adaptive scaling factor will enable the regression network to learn robust initial estimates, while CNFs refine these estimates without imposing strong dependencies during early training stages. Furthermore, the dynamic weighting ensures effective training across samples with varying uncertainties, leading to a more robust model.

Continuous Normalizing Flows Training To avoid explicitly calculating the divergence of the vector field on $z(t)$ (i.e., the trace of the Jacobian matrix) and integration, we optimize an upper bound to simplify the training:

$$\mathcal{L}_{\text{UB}} = -\log P(z(0)) + n \sup_{z(t)} \left\| \frac{\partial f(z(t), t; \theta)}{\partial z(t)} \right\|, \quad (12)$$

where n is the dimension of $z(t)$, and $\sup_{z(t)} \|\cdot\|$ denotes the Lipschitz constant of f . Inspired by Flow Matching [17], we specify an optimal transport path $z(t)$ between the initial and target distributions:

$$z(t) = (1 - (1 - \sigma_{\min})t)z(0) + tz(1), \quad (13)$$

where σ_{\min} is the standard deviation of the target distribution. The corresponding vector field is:

$$u(z(t), t) = \frac{z(1) - (1 - \sigma_{\min})z(t)}{1 - (1 - \sigma_{\min})t}. \quad (14)$$

By training $f(z(t), t; \theta)$ to match $u(z(t), t)$, the term $\sup_{z(t)} \left\| \frac{\partial f(z(t), t; \theta)}{\partial z(t)} \right\|$ approaches 0, meaning that the upper bound \mathcal{L}_{UB} approaches its minimum value. Hence the $\mathcal{L}_{\text{flow}}$ is given by (see also Lipman *et al.* [17]):

$$\mathcal{L}_{\text{flow}} = E_{t, q(\bar{x}), p(z(0))} \|f(z(t), t; \theta) - (\bar{x} - (1 - \sigma_{\min})z(0))\|^2 \quad (15)$$

Heteroscedastic Regression Network Training The regression network models the target distribution using a Laplace distribution as the reference distribution, characterized by a mean, $\hat{\mu}$ and a scale parameter, $\hat{\sigma}$. This results in the following expression for (1):

$$\mathcal{L}_{\text{reg}} = \log(\sqrt{2}\hat{\sigma}) + \frac{2|\mu_g - \hat{\mu}|}{\sqrt{2}\hat{\sigma}} \quad (16)$$

3.5 Evaluation Metrics

For 2D and 3D HPE, the primary evaluation metric is mean Average Precision (mAP). It depends not only on the localization error but also on the ranking of predictive uncertainty [7].

When predictive uncertainty is consistent with localization error in ranking, this leads to a higher mAP. To further validate the improvement on predictive uncertainty, we adopt Area under Sparsification Error (AUSE) from [9] and Area under Reliability Curve (AURG) [23]. In [16] Lind et al. demonstrate that AUSE is more robust than ranking-based UQ metrics for regression tasks.

4 Experiments

We evaluate our proposed methods on both 2D human pose in Sec. 4.1 and 3D human pose tasks Sec. 4.3.

4.1 Experiments on COCO

To demonstrate the effectiveness of our proposed method, we compare CFRE against heatmap-based methods, and state-of-the-art approaches using the COCO dataset. Our results consistently highlight the advantages of CFRE in terms of accuracy, uncertainty quantification, and computational efficiency.

Dataset We first evaluate the proposed method on a large-scale in-the-wild 2D human pose benchmark COCO-Pose [15]. This dataset provides annotations of 17 keypoints for body parts like the nose, eyes, and shoulders. It includes diverse human poses in various environments, making it a challenging yet realistic dataset. COCO is split into training, validation, and test-dev sets, with the latter excluding bounding box annotations to ensure fair evaluation and simulate real-world conditions.

Implementation Details The proposed model, CFRE, is validated on the COCO dataset using a top-down approach described in [13]. During inference, only the regression network within CFRE is utilized. The regression network consists of a backbone, an average pooling layer, and a fully connected (FC) layer. It predicts the estimated mean joint locations $\hat{\mu}$, and the standard deviation $\hat{\sigma}$ of joint locations along both axes. The output dimension is $K \times 4$, where $K = 17$ corresponds to the number of keypoints, and 4 represents $\hat{\mu}$ and $\hat{\sigma}$.

To enhance generalization, we adopt the data augmentation techniques commonly used in prior works [24]. The loss balancing weight c is set to 0.1, based on cross validation, see plot in Figure 4.

For experiments on the COCO validation set, the COCO train set is divided into 90% training and 10% validation subsets, with the COCO val set used as the test set. For evaluations on the COCO test-dev set, the entire COCO train set serves as the training set, the COCO val set is used for validation, and the COCO test-dev set is employed as the test set.

Comparison with the SotA. We compare CFRE with SOTA single-stage and two-stage methods on the COCO val and test-dev sets. We use 'ResNet-152 + FC Layer' as the architecture for our regression model, with input image resolution set to 384×233 . As shown in Tables 1 and 2, CFRE achieves competitive mAP among regression-based and heatmap-based methods. We also evaluate computational efficiency in terms of GFLOPs, where lower values indicate higher efficiency. As shown in Table 1, CFRE achieves competitive performance, outperforming SimplePose with the same backbone and approaching HRNet's performance, while requiring significantly fewer computational resources.

Qualitative Result on COCO. To compare the learned distributions qualitatively, CNFs were used to sample the model's joint location estimates, visualized as contour plots. The result is shown in Figure 3. Our proposed model was compared against heteroscedastic regression models assuming Laplace and Gaussian distributions, with CFRE sampled 200 times. The learned distribution's peak is broader than the Laplace distribution but sharper than the Gaussian, with heavier tails. The vertical variance exceeds the horizontal, indicating asymmetric spread. Moreover, it can be observed from the figure that CNFs capture more complex distributions compared to NFs.

Table 1: Comparison of different methods on COCO val.

Method	Backbone	mAP	AP_{50}	AP_{75}	AP_M	AP_L	GFLOPs
<i>Heatmap-based</i>							
Mask R-CNN [8]	Resnet-101	66.1	87.4	72.0	61.5	74.4	-
PifPaf [12]	ResNet-152	67.4	-	-	-	-	-
PersonLab [22]	ResNet-152	66.5	86.2	71.9	62.3	73.2	405.5
AE [20]	HrHRNet-W48	72.1	88.4	78.2	-	-	-
SimplePose [28]	Resnet-152	74.3	89.6	81.1	70.5	81.6	35.3
HRNet [24]	HRNet-W48	76.3	90.8	82.9	72.3	83.4	32.9
<i>Regression-based</i>							
DERK [5]	HRNet-W32	67.2	86.3	73.8	61.7	77.1	45.4
PRTR [14]	HRNet-W32	73.3	89.2	79.9	69.0	80.9	37.8
RLE [13]	Resnet-152	75.4	91.3	82.0	75.1	78.4	24.9
CFRE(Our)	Resnet-152	75.6	92.2	82.1	75.0	78.5	24.9

Table 2: Comparison of different methods on COCO test-dev.

Method	Backbone	mAP	AP_{50}	AP_{75}	AP_M	AP_L
<i>Heatmap-based</i>						
CMU-Pose [1]	3CM-3PAF	61.8	84.9	67.5	57.1	68.2
Mask R-CNN [8]	Resnet-50	63.1	87.3	68.7	57.8	71.4
RMPE [4]	PyraNet	72.3	89.2	79.1	68.0	78.6
AE [20]	Hourglass-4	65.5	86.8	72.3	60.6	72.6
PersonLab [22]	Resnet-152	68.7	89.0	75.4	64.1	75.5
SimplePose [28]	Resnet-152	73.7	91.9	81.1	70.3	80.0
Integral [25]	Resnet-101	67.8	88.2	74.8	63.9	74.0
HRNet [24]	HRNet-W48	75.5	92.5	83.3	71.9	81.5
EvoPose [19]	EvoPose2D-L	75.7	91.9	83.1	72.2	81.5
<i>Regression-based</i>						
CenterNet [29]	Hourglass-2	63.0	86.8	69.6	58.9	70.4
SPM [21]	Hourglass-8	66.9	88.5	72.9	62.6	73.1
PointSet Anchor [27]	HRNet-W48	68.7	89.9	76.3	64.8	75.3
RLE [13]	Resnet-152	74.2	89.5	80.7	71.0	79.7
CFRE(Our)	Resnet-152	73.8	89.1	80.4	70.4	80.0

4.2 Ablation Study

Firstly, we train heteroscedastic regression models only with the assumption of different distributions. We evaluate the proposed training paradigm in Sec. 3.4 and compare it with the explicit NLL training in Sec. 3.3. We also investigate the impact of the hyperparameter c , which balances the CFRE loss (10).

Comparison with Heteroscedastic Regression. We compare CFRE with heteroscedastic deep regression models assuming Gaussian and Laplace distributions. All models use the proposed architecture in Sec. 4.1, with the input size set to 384×288 , and are trained on the COCO dataset. **Results:** As shown in Table 3, Laplace-based training loss outperforms Gaussian based by 3% in mAP and

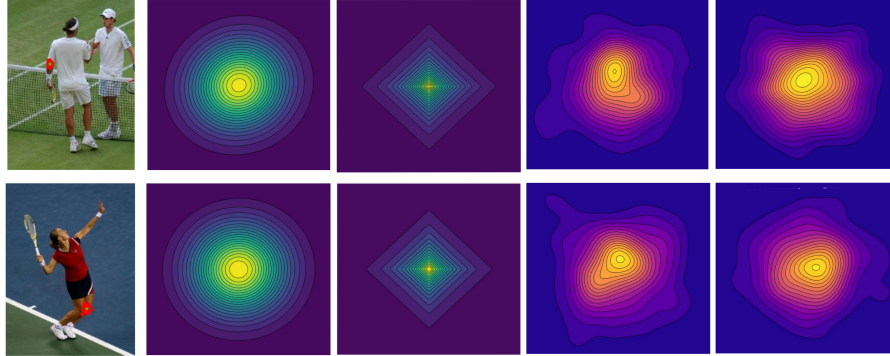


Fig. 3: Contour plot of joint estimations across multiple human instances. **First column:** Input images (Red: Samples; Green: Mean value); **Second column:** Estimation with Gaussian assumption; **Third column:** Estimation with Laplace assumption; **Fourth column:** Distributions learned by CNFs. **Fifth column:** Distributions learned by NFs. Rows correspond to different human instances and their joint estimations: (1) **left elbow**, (2) **right knee**.

lower AUSE. It suggests a better alignment between the distribution assumption and data distribution will improve performance. Furthermore, CFRE achieves a 2.4 mAP improvement over the Laplace-based model, outperforming both heteroscedastic regression models in uncertainty quantification metrics. This further validates the flexibility of our proposed architecture.

Table 3: Comparison with Heteroscedastic Regression on mAP and Uncertainty Metrics.

Method	Backbone	mAP \uparrow	PCC \uparrow	AUSE \downarrow	AURG \uparrow
heteroscedastic Regression (Gaussian)	ResNet-152	70.7	0.476	0.225	0.273
heteroscedastic Regression (Laplace)	ResNet-152	73.2	0.522	0.221	0.280
CFRE(Our)	ResNet-152	75.6	0.556	0.195	0.441

Comparison with Explicit NLL Optimization. The baseline method directly optimizes the explicit NLL formula by estimating the trace of the Jacobian matrix using the Hutchinson estimator. In contrast, CFRE leverages Flow Matching with Optimal Transport Conditional Vector Fields, bypassing the need for Jacobian trace computation and numerical integration during training.

In Table 4, we compare the two approaches on the COCO val. CFRE consistently outperforms the baseline in mAP, demonstrating the effectiveness of bypassing computational bottlenecks while maintaining high accuracy.

Effect of Hyperparameter c . The hyperparameter c in Eq. (11) determines the balance between the regression loss \mathcal{L}_{reg} and the CNF loss $\mathcal{L}_{\text{flow}}$. Figure 4 illustrates the impact of c on the COCO validation set. The model achieves peak performance when $c = 0.1$ on COCO val. Smaller values of c (e.g., $c = 0.0$) reduce

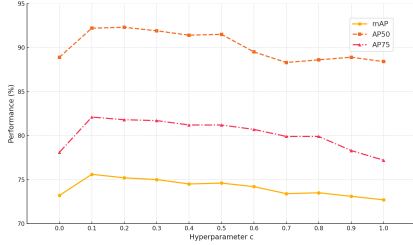


Fig. 4: Impact of Hyperparameter c on AP metrics.

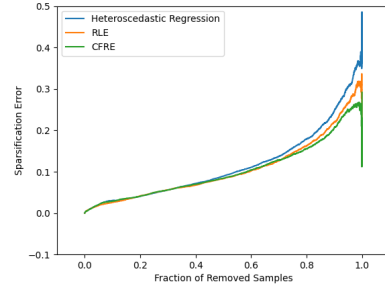


Fig. 5: Sparsification Error Plots Comparing Different Regression Methods.

Table 4: Performance Comparison of training with Explicit NLL and CFRE.

Method	Backbone	Input Size	mAP	AP ₅₀	AP ₇₅
Regression with CNF (Explicit NLL)	ResNet-50	256×192	68.0	88.7	75.1
CFRE(Our)	ResNet-50	256×192	70.7	90.5	77.1
Regression with CNF (Explicit NLL)	ResNet-152	384×288	73.8	89.1	80.0
CFRE(Our)	ResNet-152	384×288	75.6	92.2	82.2

the contribution of $\mathcal{L}_{\text{flow}}$, degrading the model to heteroscedastic regression with Laplace assumption. This study confirms that balancing the loss components through c is critical to performance, with $c = 0.1$ providing the best trade-off between regression accuracy and distribution refinement.

4.3 Experiments on Human3.6M

We further evaluate our method on the Human3.6M dataset [2, 10], a large-scale benchmark designed for 3D human pose estimation. For evaluation, we report results using metrics like Mean Per Joint Position Error (MPJPE) and Procrustes-Aligned MPJPE (PA-MPJPE) under standardized protocols. In addition, we use AUSE to report the uncertainty quantification performance of the models for 3D pose estimation tasks.

Implementation Details For the experiments conducted on the Human3.6M dataset, we adopted a single-stage approach, following the training and testing procedure of previous work [13]. The architecture used was the same as ResNet-50 with a FC layer. Input images were normalized to a size of 256×256 , and data augmentation techniques were consistent with those in previous research [13]. The initial learning rate was set to 1×10^{-3} and was decayed to 1/10 at Epochs 120 and 170. The model was trained for 200 epochs using the Adam optimizer, with a mini-batch size of 32 per GPU and a total of 2 GPUs.

Results Table 5 highlights the improvements achieved by our method on the Human3.6M dataset. Our approach achieves the lowest MPJPE (48.2 mm) and PA-MPJPE (38.2 mm), while maintaining the same GFLOPs (5.4) as RLE

Table 5: Comparison on Human3.6M

Method	#Params	GFLOPs	MPJPE ↓	PA-MPJPE ↓	AUSE ↓
Direct Regression	23.8M	5.4	50.1	39.3	0.279
Heteroscedastic Reg (Laplace)	23.8M	5.4	50.8	39.7	0.112
RLE [13]	23.8M	5.4	48.6	38.5	0.106
Regression with CFRE	23.8M	5.4	48.2	38.2	0.101

and heteroscedastic regression. In addition, our method surpasses the baseline heteroscedastic regression by 1.1% and RLE by 0.5% on AUSE.

The sparsification error plots of heteroscedastic regression, regression with RLE and CFRE are as shown in Figure 5. Sparsification error is the difference between the model sparsification curve and the oracle curve, indicating the gap between the model and the optimal uncertainty, see [16].

5 Conclusion

This study enhances regression-based Human Pose Estimation by integrating CNFs. This is shown to improve accuracy and uncertainty quantification without increasing computational costs. CNFs allow the model to dynamically learn joint location distributions, overcoming the limitations of fixed assumptions. Analysis of the learned distributions reveals sharper peaks, heavier tails, and axis-specific variances, aligning with real-world data characteristics.

The proposed model demonstrates superior performance on the COCO and Human3.6M dataset, achieving notable gains in evaluation metrics related to uncertainty such as mAP, Pearson correlation coefficient (PCC) and AUSE over traditional regression models while maintaining computational efficiency. It surpasses state-of-the-art regression methods and outperforms heatmap-based approaches with the same backbone, delivering improved accuracy at a lower computational cost. To optimize training, we derive an upper bound for the NLL of CNFs, proving its equivalence to Flow Matching training with Optimal Transport vector fields.

In summary, this work establishes CNFs as a powerful enhancement to regression-based HPE, achieving state-of-the-art results while maintaining efficiency.

Acknowledgments. This work was supported by the strategic research environment ELLIIT funded by the Swedish government, and by Vinnova, project №2023 – 02694, and Formas project №2023-00082. Computational resources were provided by the National Academic Infrastructure for Supercomputing in Sweden (NAISS), partially funded by the Swedish Research Council through grant agreement no. 2022-06725.

References

1. Cao, Z., Hidalgo, G., Simon, T., Wei, S.E., Sheikh, Y.: Openpose: Real-time multi-person 2d pose estimation using part affinity fields. *IEEE Transactions on Pattern Analysis and Machine Intelligence* **43**(1), 172–186 (2021). <https://doi.org/10.1109/TPAMI.2019.2929257>

2. Catalin Ionescu, Fuxin Li, C.S.: Latent structured models for human pose estimation. In: International Conference on Computer Vision (2011)
3. Chen, R.T.Q., Rubanova, Y., Bettencourt, J., Duvenaud, D.K.: Neural ordinary differential equations. In: Bengio, S., Wallach, H., Larochelle, H., Grauman, K., Cesa-Bianchi, N., Garnett, R. (eds.) *Advances in Neural Information Processing Systems*. vol. 31. Curran Associates, Inc. (2018)
4. Fang, H.S., Xie, S., Tai, Y.W., Lu, C.: Rmpe: Regional multi-person pose estimation. In: 2017 IEEE International Conference on Computer Vision (ICCV). pp. 2353–2362 (2017). <https://doi.org/10.1109/ICCV.2017.256>
5. Geng, Z., Sun, K., Xiao, B., Zhang, Z., Wang, J.: Bottom-up human pose estimation via disentangled keypoint regression. In: 2021 IEEE/CVF Conference on Computer Vision and Pattern Recognition (CVPR). pp. 14671–14681 (2021). <https://doi.org/10.1109/CVPR46437.2021.01444>
6. Grathwohl, W., Chen, R.T.Q., Bettencourt, J., Sutskever, I., Duvenaud, D.: FFJORD: Free-form continuous dynamics for scalable reversible generative models. <https://doi.org/10.48550/ARXIV.1810.01367>, <https://arxiv.org/abs/1810.01367>, version Number: 3
7. Gu, K., Chen, R., Yao, A.: On the calibration of human pose estimation. <https://doi.org/10.48550/ARXIV.2311.17105>, <https://arxiv.org/abs/2311.17105>, version Number: 1
8. He, K., Gkioxari, G., Dollár, P., Girshick, R.: Mask r-cnn. In: 2017 IEEE International Conference on Computer Vision (ICCV). pp. 2980–2988 (2017). <https://doi.org/10.1109/ICCV.2017.322>
9. Ilg, E., Cicek, O., Galesso, S., Klein, A., Makansi, O., Hutter, F., Brox, T.: Uncertainty estimates and multi-hypotheses networks for optical flow. In: *Proceedings of the European Conference on Computer Vision (ECCV)*. pp. 652–667 (2018)
10. Ionescu, C., Papava, D., Olaru, V., Sminchisescu, C.: Human3.6m: Large scale datasets and predictive methods for 3d human sensing in natural environments. *IEEE Transactions on Pattern Analysis and Machine Intelligence* **36**(7), 1325–1339 (jul 2014)
11. Kendall, A., Gal, Y.: What uncertainties do we need in bayesian deep learning for computer vision? <https://doi.org/10.48550/ARXIV.1703.04977>, <https://arxiv.org/abs/1703.04977>, version Number: 2
12. Kreiss, S., Bertoni, L., Alahi, A.: Pifpaf: Composite fields for human pose estimation. 2019 IEEE/CVF Conference on Computer Vision and Pattern Recognition (CVPR) pp. 11969–11978 (2019), <https://api.semanticscholar.org/CorpusID:80628362>
13. Li, J., Bian, S., Zeng, A., Wang, C., Pang, B., Liu, W., Lu, C.: Human pose regression with residual log-likelihood estimation. <https://doi.org/10.48550/ARXIV.2107.11291>, <https://arxiv.org/abs/2107.11291>, version Number: 3
14. Li, K., Wang, S., Zhang, X., Xu, Y., Xu, W., Tu, Z.: Pose recognition with cascade transformers. In: *Proceedings of the IEEE/CVF Conference on Computer Vision and Pattern Recognition (CVPR)*. pp. 1944–1953 (June 2021)
15. Lin, T.Y., Maire, M., Belongie, S.J., Bourdev, L.D., Girshick, R.B., Hays, J., Perona, P., Ramanan, D., Dollár, P., Zitnick, C.L.: Microsoft COCO: common objects in context. *CoRR* **abs/1405.0312** (2014), <http://arxiv.org/abs/1405.0312>
16. Lind, S.K., Xiong, Z., Forssén, P.E., Krüger, V.: Uncertainty quantification metrics for deep regression. *Pattern Recognition Letters* **186**, 91–97 (2024)
17. Lipman, Y., Chen, R.T.Q., Ben-Hamu, H., Nickel, M., Le, M.: Flow matching for generative modeling, <http://arxiv.org/abs/2210.02747>

18. Mathieu, M., Couprie, C., LeCun, Y.: Deep multi-scale video prediction beyond mean square error (Jan 2016), 4th International Conference on Learning Representations, ICLR 2016 ; Conference date: 02-05-2016 Through 04-05-2016
19. McNally, W., Vats, K., Wong, A., McPhee, J.: EvoPose2d: Pushing the boundaries of 2d human pose estimation using accelerated neuroevolution with weight transfer **9**, 139403–139414. <https://doi.org/10.1109/ACCESS.2021.3118207>, <https://ieeexplore.ieee.org/document/9559918/>
20. Newell, A., Huang, Z., Deng, J.: Associative embedding: End-to-end learning for joint detection and grouping. In: Guyon, I., Luxburg, U.V., Bengio, S., Wallach, H., Fergus, R., Vishwanathan, S., Garnett, R. (eds.) *Advances in Neural Information Processing Systems*. vol. 30. Curran Associates, Inc. (2017)
21. Nie, X., Feng, J., Zhang, J., Yan, S.: Single-stage multi-person pose machines. In: 2019 IEEE/CVF International Conference on Computer Vision (ICCV). pp. 6950–6959 (2019). <https://doi.org/10.1109/ICCV.2019.00705>
22. Papandreou, G., Zhu, T., Chen, L.C., Gidaris, S., Tompson, J., Murphy, K.: Personlab: Person pose estimation and instance segmentation with a bottom-up, part-based, geometric embedding model. In: *Computer Vision – ECCV 2018*. pp. 282–299. Springer International Publishing, Cham (2018)
23. Poggi, M., Aleotti, F., Tosi, F., Mattoccia, S.: On the uncertainty of self-supervised monocular depth estimation. <https://doi.org/10.48550/ARXIV.2005.06209>, <https://arxiv.org/abs/2005.06209>, version Number: 1
24. Sun, K., Xiao, B., Liu, D., Wang, J.: Deep high-resolution representation learning for human pose estimation, <http://arxiv.org/abs/1902.09212>
25. Sun, X., Xiao, B., Wei, F., Liang, S., Wei, Y.: Integral human pose regression. In: Ferrari, V., Hebert, M., Sminchisescu, C., Weiss, Y. (eds.) *Computer Vision – ECCV 2018*. pp. 536–553. Springer International Publishing, Cham (2018)
26. Tompson, J.J., Jain, A., LeCun, Y., Bregler, C.: Joint training of a convolutional network and a graphical model for human pose estimation. In: Ghahramani, Z., Welling, M., Cortes, C., Lawrence, N., Weinberger, K. (eds.) *Advances in Neural Information Processing Systems*. vol. 27. Curran Associates, Inc. (2014)
27. Wei, F., Sun, X., Li, H., Wang, J., Lin, S.: Point-set anchors for object detection, instance segmentation and pose estimation. In: Vedaldi, A., Bischof, H., Brox, T., Frahm, J.M. (eds.) *Computer Vision – ECCV 2020*. pp. 527–544. Springer International Publishing, Cham (2020)
28. Xiao, B., Wu, H., Wei, Y.: Simple baselines for human pose estimation and tracking. In: Ferrari, V., Hebert, M., Sminchisescu, C., Weiss, Y. (eds.) *Computer Vision – ECCV 2018*. pp. 472–487. Springer International Publishing, Cham (2018)
29. Zhou, X., Wang, D., Krähenbühl, P.: Objects as points. <https://doi.org/10.48550/ARXIV.1904.07850>, <https://arxiv.org/abs/1904.07850>, version Number: 2

Supplementary Material for the Paper: Continuous Normalizing Flows for Uncertainty-Aware Human Pose Estimation

1 Theorem Proof

Theorem 1: For an $n \times n$ matrix A , the inequality $\text{tr}(A) \leq \sqrt{n}\|A\|_F$ holds, where $\|A\|_F$ is the Frobenius norm of the matrix A .

Proof:

$$\text{tr}(A) = \sum_{i=1}^n A_{ii} \leq \sqrt{n} \left(\sum_{i=1}^n A_{ii}^2 \right)^{\frac{1}{2}} \quad (\text{Cauchy-Schwarz inequality}) \quad (1)$$

$$\leq \sqrt{n} \left(\sum_{i=1}^n \sum_{j=1}^n |A_{ij}|^2 \right)^{\frac{1}{2}} \quad (2)$$

$$= \sqrt{n}\|A\|_F. \quad (3)$$

Theorem 2: For an $n \times n$ matrix A , the inequality $\|A\|_F \leq \sqrt{n}\|A\|$ holds, where $\|A\|_F$ is the Frobenius norm of the matrix A and $\|A\|$ is the spectral norm of this matrix.

Proof:

$$\|A\| = \max_{\|x\|_2=1} \|Ax\|_2 = \sigma_{\max}(A) = \max_{1 \leq i \leq n} \sigma_i, \quad (4)$$

where $\sigma_{\max}(A)$ represents the largest singular value of A , $\sigma_i(A)$ are the singular values of A . Frobenius norm of A : $\|A\|_F = \sqrt{\text{tr}(A^*A)} = \sqrt{\sum_{i=1}^n \sigma_i^2(A)}$.

Since $\sigma_i \leq \sigma_{\max}(A)$ for all i , we have $\sum_{i=1}^n \sigma_i^2 \leq \sum_{i=1}^n \sigma_{\max}(A)^2 = n \cdot \sigma_{\max}(A)^2 = n\|A\|^2$.

Hence, $\|A\|_F \leq \sqrt{n}\|A\|$.

Theorem 3: Consider a function $f(z) : \mathbb{R}^n \rightarrow \mathbb{R}^n$ with partial derivatives of z everywhere so that the Jacobian matrix is well-defined. Assume $f(z)$ is **Lipschitz continuous** on z . Let $L \geq 0$ be its **Lipschitz constant**. Then $\left\| \frac{\partial f}{\partial z} \right\| \leq L, \forall z$, where $\|\cdot\|$ denotes the spectral matrix norm.

Proof:

For a fixed $\delta > 0$, $z \in \mathbb{R}^n$, and assuming that the derivative $\frac{\partial f}{\partial z}$ exists, let L be the Lipschitz constant of f . Hence, f is $(L + \delta)$ -Lipschitz continuous. Let $\forall v \in \mathbb{R}^n$ with $\|v\| = 1$ be a unit vector. Consider the quantity:

$$\frac{|f(x) - f(x + tv)|}{t}, \quad (5)$$

where $t \in \mathbb{R}$. When $t \rightarrow 0$, $J_f(x)(v)$ is the directional derivative of f in the direction v . Thus, there exists $\epsilon_v > 0$ such that:

$$\frac{|f(x) - f(x + tv)|}{t} < L + \delta, \quad \text{for } |t| < \epsilon_v. \quad (6)$$

By the compactness of the unit sphere, there exists a common $\epsilon > 0$ such that

$$\frac{|f(x) - f(z)|}{|x - z|} < L + \delta, \quad \text{if } |x - z| < \epsilon. \quad (7)$$

Consider the line segment connecting the points x and y , covered and divided into a finite number of N small intervals by a series of balls $\{B_1, \dots, B_N\}$, where f is $(L + \delta)$ -Lipschitz continuous on each ball, and the centers of these balls lie on the line segment. Adjacent balls intersect each other, so for the center point x_i of the i -th ball, we have

$$|f(x_{i+1}) - f(x_i)| \leq (L + \delta)|x_{i+1} - x_i|. \quad (8)$$

Applying the triangle inequality,

$$|f(x) - f(y)| = |f(x_N) - f(x_1)| \quad (9)$$

$$\leq \sum_{i=1}^N |f(x_{i+1}) - f(x_i)| \quad (10)$$

$$\leq (L + \delta) \sum_{i=1}^N |x_{i+1} - x_i| \quad (11)$$

$$= (L + \delta)|x - y|. \quad (12)$$

By using more balls to cover the line segment, we can let $\delta \rightarrow 0$, so

$$J_f(x)(v) = \lim_{t \rightarrow 0} \frac{|f(x) - f(x + tv)|}{t} \leq L, \quad (13)$$

thus,

$$\left\| \frac{\partial f}{\partial z} \right\| = \|J_f(x)\| = \sup_{\substack{v \in \mathbb{R}^n \\ \|v\|=1}} J_f(x)(v) \leq L. \quad (14)$$

This result is trivial when $n = 1$. we can use the definition of the derivative and the mean value theorem to obtain the conclusion of the theorem 3. In the proof above, we have extended it to higher dimensions.

2 The derivation of upper bound

In order to make the CNFs model trainable, we consider optimizing the upper bound of \mathcal{L}_{NLL} . Consider the term $\text{tr}(\frac{\partial f(z(t), t; \theta)}{\partial z(t)})$, by applying Theorem 1, we have

$$\text{tr}(\frac{\partial f(z(t), t; \theta)}{\partial z(t)}) \leq \sqrt{n} \left\| \frac{\partial f(z(t), t; \theta)}{\partial z(t)} \right\|_F, \quad (15)$$

where n is the dimension of the Jacobian matrix of $f(z(t), t; \theta)$ on $z(t)$. By applying Theorem 2, we have

$$\left\| \frac{\partial f(z(t), t; \theta)}{\partial z(t)} \right\|_F \leq \sqrt{n} \left\| \frac{\partial f(z(t), t; \theta)}{\partial z(t)} \right\|. \quad (16)$$

Hence,

$$\text{tr}(\frac{\partial f(z(t), t; \theta)}{\partial z(t)}) \leq \sqrt{n} \left\| \frac{\partial f(z(t), t; \theta)}{\partial z(t)} \right\|_F \leq n \left\| \frac{\partial f(z(t), t; \theta)}{\partial z(t)} \right\|. \quad (17)$$

Previously, we assumed that $f(z(t), t; \theta)$ is uniformly Lipschitz continuous in $z(t)$. Also the function $z(t)$ is continuous and everywhere differentiable on t . From Theorem 4, for $\forall f(z(t), t; \theta)$ uniformly Lipschitz continuous in $z(t)$, $\exists L_\theta \in \mathbb{R}$ and $L_\theta \geq 0$:

$$\left\| \frac{\partial f(z(t), t; \theta)}{\partial z(t)} \right\| \leq L_\theta, \quad (18)$$

where θ is the parameter of f . Also, we have

$$\text{tr}(\frac{\partial f(z(t), t; \theta)}{\partial z(t)}) \leq n \left\| \frac{\partial f(z(t), t; \theta)}{\partial z(t)} \right\|, \quad (19)$$

hence,

$$\int_0^1 \text{tr}(\frac{\partial f(z(t), t; \theta)}{\partial z(t)}) dt \leq n \int_0^1 \left\| \frac{\partial f(z(t), t; \theta)}{\partial z(t)} \right\| dt \leq nL_\theta. \quad (20)$$

Also recall f is uniformly Lipschitz continuous, hence there exists a minimal Lipschitz constant:

$$\widehat{L}_\theta = \sup_{z(t)} \left\| \frac{\partial f(z(t), t; \theta)}{\partial z(t)} \right\|. \quad (21)$$

Therefore \mathcal{L}_{NLL} exists an upper bound:

$$\mathcal{L}_{\text{UB}} = -\log p(z(0)) + n \sup_{z(t)} \left\| \frac{\partial f(z(t), t; \theta)}{\partial z(t)} \right\|. \quad (22)$$

It is not difficult to find that our optimization goal is mainly determined by \widehat{L}_θ . Also, the spectral norm of all matrix is always non-negative. Therefore, when $\sup_{z(t)} \left\| \frac{\partial f(z(t), t; \theta)}{\partial z(t)} \right\| = 0$, the upper bound \mathcal{L}_{UB} reaches its minimum value.